Orientation-dependent electromechanical properties of Mn-doped (Li,Na,K)(Nb,Ta)O_3 single crystals

Hairui Liu, Jurij Koruza, Philippe Veber, Daniel Rytz, Mario Maglione, Jürgen Rödel

AIP Applied Physics Letters

Orientation-dependent electromechanical properties of Mn-doped (Li,Na,K)(Nb,Ta)O3 single crystals

Hairui Liu, Jurij Koruza, Philippe Veber, Daniel Rytz, Mario Maglione, and Jürgen Rödel

Citation: Applied Physics Letters **109**, 152902 (2016); doi: 10.1063/1.4964465
View online: http://dx.doi.org/10.1063/1.4964465
View Table of Contents: http://scitation.aip.org/content/aip/journal/apl/109/15?ver=pdfcov
Published by the AIP Publishing

Orientation-dependent electromechanical properties of Mn-doped (Li,Na,K)(Nb,Ta)O_3 single crystals

Hairui Liu,[1,2,3,a)] Jurij Koruza,[1] Philippe Veber,[2,3] Daniel Rytz,[4] Mario Maglione,[2,3] and Jürgen Rödel[1]
[1]*Institute of Materials Science, Technische Universität Darmstadt, Alarich-Weiss-Straße 2, Darmstadt 64287, Germany*
[2]*CNRS, ICMCB, UPR 9048, Pessac 33600, France*
[3]*Université de Bordeaux, ICMCB, UPR 9048, Pessac 33600, France*
[4]*FEE GmbH, Struthstr. 2, Idar-Oberstein 55743, Germany*

(Received 6 July 2016; accepted 26 September 2016; published online 10 October 2016)

Orientation and temperature dependence of dielectric and electromechanical properties of Mn-doped (Li,Na,K)(Nb,Ta)O_3 single crystals were investigated. Samples exhibited very low dielectric losses, with tanδ between 0.03 and 0.05 over a broad temperature range between room temperature and 480 °C. Influences of the crystallographic structure and external electric field on polarization and strain parameters are discussed. The orientation-dependent electrical properties were ascribed to the anisotropic polarization rotation in the crystals. Higher maximum polarization, coercive field, and negative strain were achieved when the electric field was oriented along one of the spontaneous polarization directions. The highest maximum unipolar strain of 0.42% (at 3 kV/mm) and the normalized strain d_{33}^* of 1391 pm/V were obtained in the $[001]_{PC}$-oriented sample at 100 °C, which was much higher than the values obtained for the $[110]_{PC}$-oriented sample. Further insight of the phase transition behavior is given by comparing the temperature-dependence of the small- and large-signal dielectric and piezoelectric properties. The observed changes are rationalized by the different increase rates of the dielectric permittivity and piezoelectric coefficients with temperature. *Published by AIP Publishing*. [http://dx.doi.org/10.1063/1.4964465]

Ferroelectric and piezoelectric materials have been widely investigated due to their potential application as sensors, actuators, and transducers.[1] In most perovskite ferroelectric systems, enhanced piezoelectric properties are observed at structural phase boundaries, originating from the flattened free energy surface.[2] Several mechanisms have been proposed to explain this behaviour, including coexistence of mixed phases at morphotropic (MPB)[3] or polymorphic (PPT)[4] phase boundaries, existence of intermediate monoclinic phases,[5–8] presence of nanodomains,[9] electric-field (E)-induced phase transitions[10] and polarization extension.[6,11] Most of these mechanisms are related to the rotation of the polarization vector from one spontaneous polarization (P_S) direction to another with an external electric or mechanical field stimulus.[12] This includes two domain switching types: 180° and non-180°. The former is only ferroelectric and includes negligible mechanical strain, while the latter additionally involves ferroelasticity.[13]

Investigation of the single crystalline material form offers a pathway for understanding the underlying mechanisms of the enhanced electromechanical properties. Orientation dependence of electrical properties has been extensively studied in many ferroelectric crystals, such as $Pb(Mb_{1/3}Nb_{2/3})O_3$-$PbTiO_3$ (PMN-PT),[14] NBT,[15] $BaTiO_3$,[16] $(Na,K)_{0.5}Bi_{0.5}TiO_3$,[17] and NBT-BT.[18,19] A study of undoped $(Na,K)NbO_3$ (KNN) crystals along $[001]_{PC}$ and $[110]_{PC}$ orientations at room temperature was reported by Deng *et al.*,[20] whereby the maximum E-field-induced bipolar strain at 2 kV/mm was about 0.025% along both orientations, which is lower as compared to PMN-PT crystals. Influences of polarization rotation on the electromechanical properties of KNN-based single crystals, one of the promising lead-free piezoelectric systems,[21,22] have not been explored so far.

The high leakage currents[23–25] and high dielectric losses,[26,27] probably induced by the volatilization of alkali elements,[28] the appearance of Nb^{4+} ions,[29] and the segregation phenomena[30] during the crystal growth process, often prevent the detailed characterization of the electromechanical properties and stunt further development of KNN-based crystals. The partial substitution of Nb with Mn was reported to effectively suppress leakage currents.[29] Lin *et al.*[31] obtained a much lower leakage current density and a larger piezoelectric constant d_{33} of 0.5 mol. % MnO_2-doped KNN crystals, as compared to undoped KNN crystals. Moreover, the recent work on Mn-doped (Li,Na,K)(Nb,Ta)O_3 (Mn-doped KNLTN) single crystals by Huo *et al.*[32] revealed a high d_{33} of 630 pC/N, which can compete with lead-based piezoelectrics. However, information about the influences of the crystallographic structure and orientation on electrical properties of KNN-based single crystals is still missing.

In this work, we investigated the temperature-dependent dielectric and electromechanical performance of Mn-doped KNLTN single crystals with two different crystallographic symmetries and two orientations, in order to understand the interrelationship between inherent anisotropy and electrical properties.

Mn-doped KNLTN crystals were grown by the self-flux solution method, using a Pt spatula as a preferential nucleation site. The polycrystalline precursor with the formula

[a)]Author to whom correspondence should be addressed. Electronic mail: liu@ceramics.tu-darmstadt.de

$(Li_{0.15}Na_{0.1074}K_{0.7426}Nb_{0.9921}Ta_{0.0079})O_3$ and 1 mol. % MnO_2 was prepared by weighing, mixing, and calcining the high purity (99.99%) raw materials of MnO_2, K_2CO_3, Na_2CO_3, Li_2CO_3, Nb_2O_5, and Ta_2O_5 in a Pt crucible. The batch was heated to above 1200 °C and held at a soaking temperature of about 20 °C above the saturation temperature while being stirred continuously. The crystal growth was carried out using a Pt spatula as the nucleation active center in a resistive heating furnace with a small longitudinal thermal gradient (<1 °C/mm). Details about the crystal growth can be obtained in Refs. 33 and 34. Crystallographic orientations were determined by Laue backscattering. The crystallographic structure was analyzed on crushed single crystals by a powder X-ray diffraction (PANalytical X'pert Pro MPD diffractometer) with Cu-K_α radiation. Two parallel flat surfaces were painted with silver electrodes. Temperature-dependent dielectric properties were measured by a HP 4284A LCR meter. Ferroelectric hysteresis polarization (*P-E*) and strain curves (*S-E*) were measured as a function of temperature using an aixACCT TF ferroelectric analyzer (Aachen, Germany). A triangular electric field signal was selected. The measured frequencies of bipolar and unipolar curves were 1 Hz and 2 Hz, respectively. The temperature-dependent small signal d_{33} coefficient was measured by a Polytec laser Doppler vibrometer, while exciting the sample with a 10 V sinusoidal AC signal with a frequency of 1 kHz.

Fig. 1(a) provides the XRD pattern of the crushed Mn-doped KNLTN crystal at room temperature. A pure orthorhombic perovskite structure without any secondary phase was detected. The inset of Fig. 1(a) presents the photograph of the as-grown crystal boule. The composition, measured by electron probe micro-analysis and inductively coupled plasma optical emission spectroscopy, was $(Li_{0.03}Na_{0.33}K_{0.64})((Nb_{0.98}Ta_{0.02})_{99.97\%}Mn_{0.03\%\pm0.02\%})O_{3-\delta}$, which differs from the starting formula due to segregation phenomena. A detailed description of the segregation and the composition analysis can be found in Ref. 30. Note that the as-grown crystal boule had a yellow color, characteristic of the Mn-doped KNLTN, while the slight color gradient might originate from ferroelectric domains, as previously described by Inagaki *et al.*[35]

Fig. 1(b) reveals the temperature-dependent dielectric permittivity and losses for $[001]_{PC}$ and $[110]_{PC}$-oriented Mn-doped KNLTN crystals at 100 kHz during heating and cooling. Two anomalies were observed: the one at higher temperature was identified as the Curie temperature (T_C), corresponding to the tetragonal-cubic phase transition, while the other one at lower temperature refers to the orthorhombic-tetragonal ($T_{O\text{-}T}$) transition.[36] The T_C and $T_{O\text{-}T}$ of both $[001]_{PC}$ and $[110]_{PC}$ orientations during cooling are (442 °C, 102 °C) and (441 °C, 100 °C), respectively. During heating, these values are (450 °C, 123 °C) and (449 °C, 124 °C). The thermal hysteresis indicates that both transitions are of first-order.[37] The differences of phase transition temperatures between two orientations are within the measurement error, indicative of orientation-independent phase transition temperatures. It is also noted that the dielectric losses are very low due to doping with Mn, even at temperatures above 450 °C.

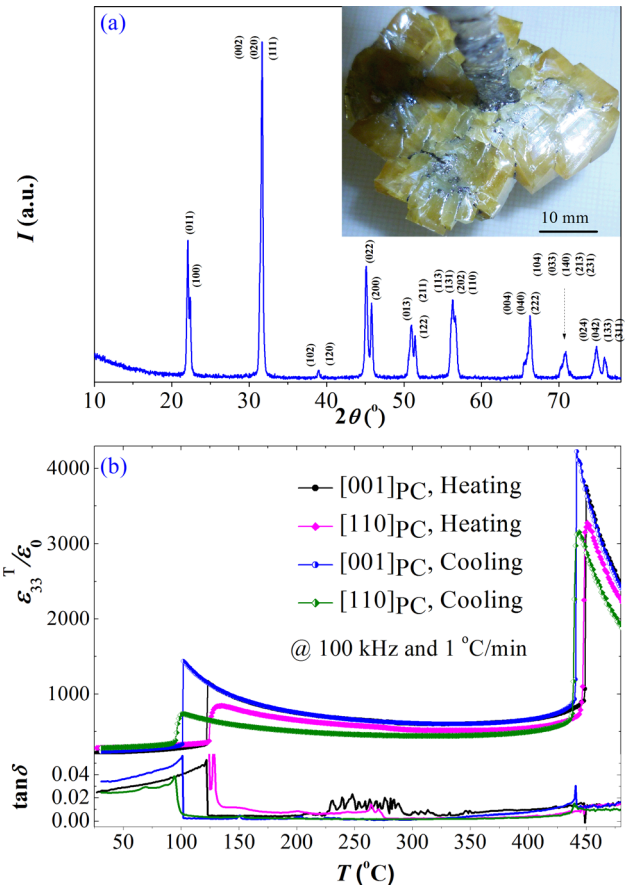

FIG. 1. (a) XRD pattern of the crushed Mn-doped KNLTN crystal at room temperature and (b) temperature-dependent dielectric permittivity and losses of $[001]_{PC}$ and $[110]_{PC}$-oriented Mn-doped KNLTN samples during heating and cooling. The inset in (a) is the photograph of the as-grown single crystal boule.

Figs. 2(a)–2(d) display *P-E* loops of $[001]_{PC}$ and $[110]_{PC}$-oriented Mn-doped KNLTN single crystals measured at 3 kV/mm at various temperatures. Typical rectangular *P-E* loops are observed for both orientations below 100 °C (Figs. 2(a) and 2(b)). When the temperature is close to 100 °C, the *P-E* loops get distorted and the one measured along the $[110]_{PC}$ orientation is pinched at lower fields. This type of pinched *P-E* loop might result from the difficulty in achieving a fully poled state along the $[110]_{PC}$ orientation for tetragonal domains. However, further studies are required to fully understand the observed pinching of the *P-E* loop at the transition temperature. Figs. 3(a)–3(c) summarize the maximum polarization P_{max}, remanent polarization P_r, and the coercive field E_C. For both orientations, P_{max} and P_r decrease with increasing temperature and exhibit a sharp drop near 100 °C, while E_C first decreases and then increases remarkably when the temperature is close to 100 °C. This temperature corresponds to the orthorhombic-tetragonal phase transition, as seen in Fig. 1(b). Above 100 °C, E_C of both orientations remains stable. The gradual decrease of P_{max}, P_r, and E_C with increasing temperature within the single-phase range, either orthorhombic or tetragonal, is related to the increased thermal oscillations and decreased lattice distortions.

In Figs. 3(a)–3(c), the orthorhombic phase reveals higher P_{max} and P_r but lower E_C, as compared to the tetragonal phase, which was previously reported by Huan *et al.*[38] This is attributed to the larger number of P_S vectors and

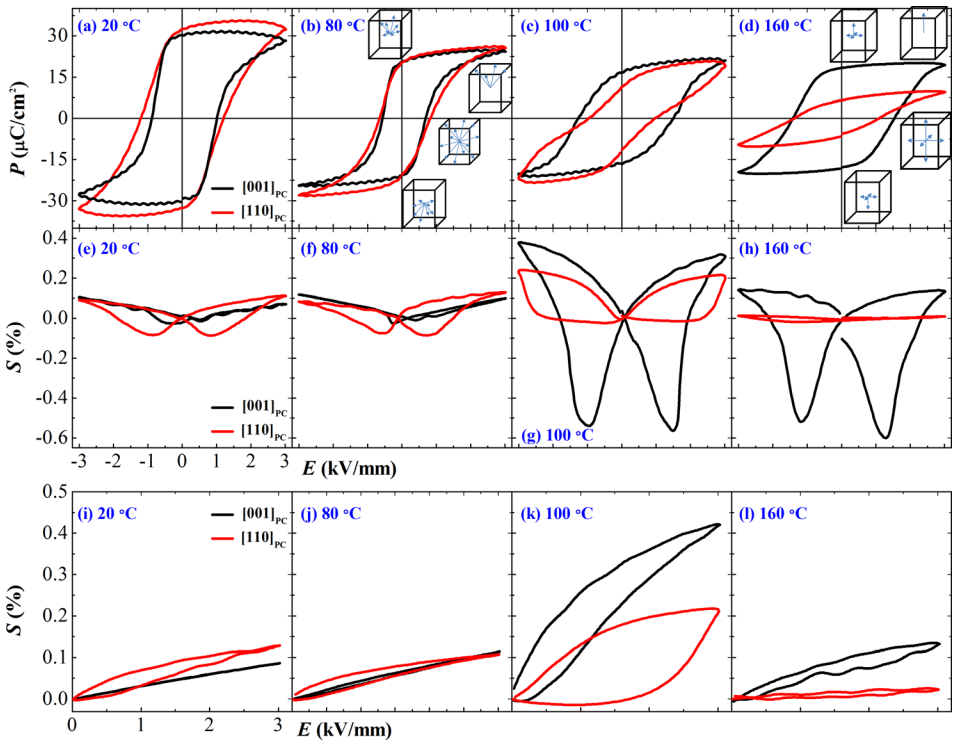

FIG. 2. Temperature-dependent (a)–(d) bipolar *P-E*, (e)–(h) *S-E*, and (i)–(l) unipolar *S-E* curves of $[001]_{PC}$ and $[110]_{PC}$-oriented Mn-doped KNLTN samples. The insets in (b) and (d) provide the possible domain orientations from $0 \rightarrow E_C \rightarrow E_{max} \rightarrow 0$ for the $[001]_{PC}$ oriented sample in the orthorhombic ($E \nparallel P_S$) and the tetragonal ($E \| P_S$) phase.

lower symmetry of the orthorhombic phase.[39] The higher E_C in the tetragonal phase in the vicinity of $T_{O\text{-}T}$ can be explained by the higher lattice distortion of the tetragonal structure, as compared to the orthorhombic one.[40] Furthermore, while the 90° domain switching can occur in both phases, the 60° domain switching only happens in the orthorhombic phase, which additionally lowers the E_C.

Figs. 3(a)–3(c) also indicate that in the orthorhombic phase, the highest values of P_{max}, P_r, and E_C were obtained for the $[110]_{PC}$ orientation, while in the tetragonal phase, the highest values for these parameters were found along the $[001]_{PC}$ direction. This gives an indication of the relationship between ferroelectric response and the *E*-field direction. It is well known that the spontaneous polarizations (P_S) of the orthorhombic phase are along $\langle 110 \rangle_{PC}$ directions (12 equivalent P_S) and that of the tetragonal phase are along $\langle 001 \rangle_{PC}$ directions (6 equivalent P_S). It can therefore be concluded that P_{max}, P_r, and E_C are the largest when *E*-field is parallel to one of the P_S directions ($E \| P_S$). This is due to the higher possibility to achieve a single-domain state at E_{max} when $E \| P_S$. If *E*-field is not parallel to any of the P_S ($E \nparallel P_S$), dipoles at E_{max} cannot align, resulting in a multi-domain instead of single-domain state. After the field removal, both $E \| P_S$ and $E \nparallel P_S$ cases exhibit a multi-domain state. The higher P_r for $E \| P_S$ corresponds to the orientation independence of backswitching in KNN-based single crystals. This can be indicated by Figs. 3(a) and 3(b), which display a similar decrease in polarization from P_{max} to P_r for two orientations in either orthorhombic or tetragonal phase.

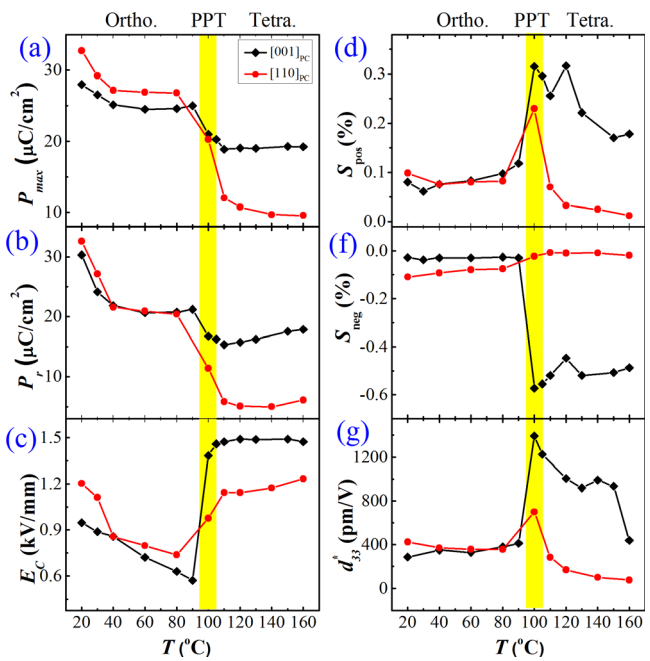

FIG. 3. Temperature-dependent (a) P_{max}, (b) P_r, (c) E_C, (d) bipolar S_{pos} and (f) S_{neg}, and (g) d_{33}^* values of $[001]_{PC}$ and $[110]_{PC}$-oriented Mn-doped KNLTN samples.

Figs. 2(e)–2(h) display the temperature-dependent bipolar *S-E* curves for both orientations. The corresponding unipolar *S-E* curves are depicted in Figs. 2(i)–2(l). The temperature dependence of the maximum bipolar positive strain S_{pos} and negative strain S_{neg} are plotted in Figs. 3(d) and 3(f). In addition, the normalized strain d_{33}^*, calculated from unipolar measurements as S_{max}/E_{max}, are presented in Fig. 3(g). The highest values for S_{pos}, S_{max}, and d_{33}^* are reached at 100 °C: 0.31%, 0.42%, 1391 pm/V for $[001]_{PC}$ and 0.21%, 0.21%, 700 pm/V for $[110]_{PC}$-oriented samples. Above $T_{O\text{-}T}$, S_{pos} and d_{33}^* become smaller for both orientations with increasing temperature. The absolute value of S_{neg} along the $[001]_{PC}$ orientation is relatively small at low temperatures, but increases sharply to 0.56% at $T_{O\text{-}T}$ (Fig. 3(f)). On the other hand, the absolute value of S_{neg} along the $[110]_{PC}$ orientation is gradually reduced upon heating and

becomes negligible above $T_{O\text{-}T}$. In addition, both S_{pos} and S_{neg} reduce slightly along the $[001]_{PC}$ direction above $T_{O\text{-}T}$, but the latter is interestingly still higher than the former. The relatively good thermal stability and high values of S_{pos} and S_{neg} indicate the high potential of these crystals for piezoelectric applications if $T_{O\text{-}T}$ is shifted to room temperature, which can be easily achieved by changing the Ta content.[30]

The orientation dependence of E_C and S_{neg} of the Mn-doped KNLTN crystal in a single-phase region is observed in Figs. 3(c) and 3(f), originating from the different contributions of non-180° and 180° domain switching events during increasing E from 0 to E_C.[41] For tetragonal phases, the probability of non-180° domain switching is approximately 4/6 if $E \| P_S$ ($[001]_{PC}$), but only 2/6 if $E \nparallel P_S$ ($[110]_{PC}$). For orthorhombic phases, this probability is about 10/12 when $E \| P_S$ ($[110]_{PC}$) and 4/12 when $E \nparallel P_S$ ($[001]_{PC}$). Thus, non-180° domain switching events are dominant for the $E \| P_S$ case, while the 180° events are dominant for $E \nparallel P_S$, when E is increased from 0 to E_C. Since non-180° switching creates strain and 180° switching does not, higher S_{neg} can be observed when $E \| P_S$.

While the temperature-dependent changes of the polarization and strain within the single-phase regions follow the expected trends, the behavior observed near the phase transition temperature is less intuitive. The observed large field-induced S_{pos} of the $[001]_{PC}$-oriented sample (Figs. 2(g) and 2(k)) would suggest a correspondingly large field-induced change in the polarization, following the fundamental equation relating to E-field-induced polarization and strain:

$$S_{ij} = Q_{ijkl} \cdot P_k \cdot P_l, \tag{1}$$

where S_{ij} is the strain tensor, Q_{ijkl} is the electrostrictive coefficient tensor, and P_k and P_l are the polarization components. However, the field-induced polarization change (P_{max} - P_r) at the phase transition temperature was found to be negligible, as compared to the E-field-induced strain (Fig. 4(a)). The observed difference implies a large increase of the electrostrictive coefficient Q. Similar phenomena were previously observed in other ferroelectric single crystals.[14] At this point, we should note that the calculation of electrostrictive coefficients of our samples failed due to their relatively low breakdown fields, which prevented sufficient saturation of the loops. The E-field-induced electric displacement D_i and strain S_{ij} in the non-linear large-signal regime can be described by the following equations (for zero stress):[42]

$$D_i = \varepsilon_{ij} E_j + \varepsilon_{ijk} E_j E_k + \cdots \tag{2}$$

$$S_{ij} = d_{ijk} E_k + M_{ijkl} E_k E_l + \cdots \tag{3}$$

where M_{ijkl} is another electrostrictive coefficient tensor, related to Q_{ijkl} by the permittivity, ε_{ij} and ε_{ijk} are the permittivity tensors, d_{ijk} is the piezoelectric coefficient tensor, and E_k and E_l are the E-field vectors. Note that in most ferroelectrics, $D_i \approx P_i$ due to the large permittivity values. Fig. 4(b) features the temperature dependence of the changes in small signal d_{33} and ε_{33} of the $[001]_{PC}$-oriented sample. The decreased d_{33} above $T_{O\text{-}T}$ indicates depolarization. Both parameters were found to increase upon heating from room temperature towards the $T_{O\text{-}T}$, as expected for a ferroelectric-

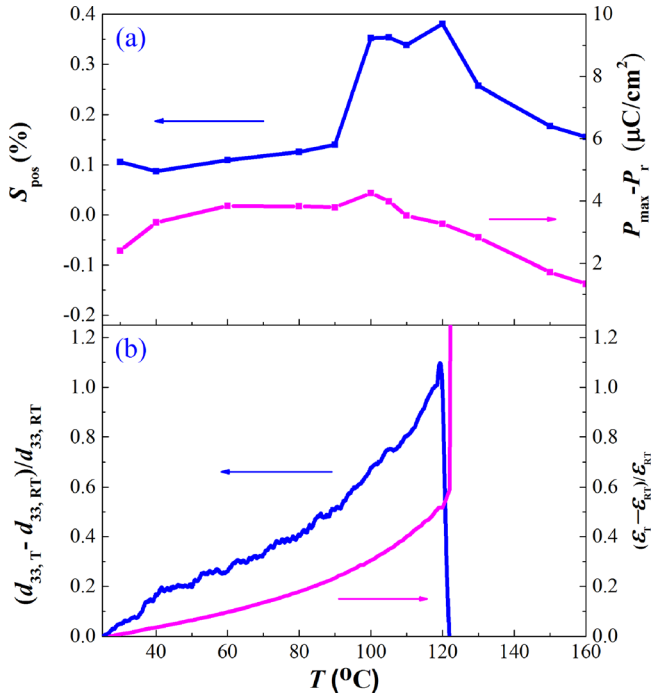

FIG. 4. Temperature-dependent properties of the $[001]_{PC}$-oriented sample: (a) large signal S_{pos} and (P_{max}-P_r), and (b) small signal d_{33} and permittivity values, normalized with respect to the room temperature value.

ferroelectric structural phase transition. However, the rate of increase of the piezoelectric coefficient is larger, as compared to the one, of the dielectric permittivity. This difference is believed to be the main origin of the larger increase of the E-field-induced strain at $T_{O\text{-}T}$, which depends predominantly on piezoelectric and electrostrictive coefficient tensors (Eq. (3)), while the polarization is related only to the permittivity (Eq. (2)). Note that the small signal d_{33} and ε_{33} were used for the comparison here and the temperature dependence of both parameters is expected to display similar trends under large E-fields.

Interestingly, the electromechanical strains (bipolar S_{pos} and unipolar S_{max}) in the vicinity of $T_{O\text{-}T}$ along the $[001]_{PC}$ orientation are much larger than those along the $[110]_{PC}$ orientation (yellow regions in Figs. 3(d) and 3(g)). A similar observation was reported for NBT-BT crystals by Ge *et al.*[43] This phenomenon can be described as follows. For the $[001]_{PC}$–oriented sample, no polarization aligns with E-field below $T_{O\text{-}T}$. When temperature approaches $T_{O\text{-}T}$, the coexisting structure of orthorhombic and tetragonal phases drives polarizations to rotate to the E-field direction. For the $[110]_{PC}$–oriented sample, some polarization vectors align with E-field below $T_{O\text{-}T}$. When temperature reaches $T_{O\text{-}T}$, the majority of polarization vectors can be driven to rotate from $\langle 110 \rangle_{PC}$ to $\langle 001 \rangle_{PC}$ and some remain aligned with E-field. This hypothesis should be further verified by synchrotron XRD and phenomenological calculations.

In summary, $(Li_{0.03}Na_{0.33}K_{0.64})((Nb_{0.98}Ta_{0.02})_{99.97\%}Mn_{0.03\%\pm0.02\%})O_{3-\delta}$ single crystals with high electromechanical properties were investigated along $[001]_{PC}$ and $[110]_{PC}$ orientations in a broad temperature range. These electrical properties are dependent on the relative direction between the electric field and spontaneous polarization vectors. For $E \| P_S$, higher P_{max}, P_r, E_C and S_{neg} values can be achieved,

due to the different polarization rotation paths. In addition, the *E*-field-induced strain near $T_{O\text{-}T}$ of the $[001]_{PC}$ orientation was higher than that of the $[110]_{PC}$ sample. The differences in the large-signal polarization and strain response in the vicinity of the $T_{O\text{-}T}$ are related to different rates of the change of permittivity and piezoelectric coefficients with temperature.

See supplementary material for the temperature-dependent permittivity and dielectric losses of the $[001]_{PC}$ and $[110]_{PC}$-oriented Mn-doped KNLTN samples at 10 kHz, 100 kHz and 1 MHz.

The authors are thankful for the financial support from the Erasmus Mundus International Doctoral School IDS-FunMat under the Project No. 2013-07 and German-French Doctoral School. The authors would like to thank Professor George Rossetti, Jr. for his valuable discussions.

[1]N. Setter, *Piezoelectric Materials in Devices* (Swiss Federal Institute of Technology, Lausanne, 2002).
[2]A. A. Heitmann and G. A. Rossetti, J. Am. Ceram. Soc. **97**(6), 1661 (2014).
[3]B. Jaffe, W. R. Cook, and H. Jaffe, *Piezoelectric Ceramics* (Academic Press Inc., New York, 1971).
[4]E. K. Akdoğan, K. Kerman, M. Abazari, and A. Safari, Appl. Phys. Lett. **92**(11), 112908 (2008).
[5]H. Fu and R. E. Cohen, Nature **403**(6767), 281 (2000).
[6]D. Damjanovic, Appl. Phys. Lett. **97**(6), 062906 (2010).
[7]B. Noheda, D. Cox, G. Shirane, S.-E. Park, L. Cross, and Z. Zhong, Phys. Rev. Lett. **86**(17), 3891 (2001).
[8]L. Fan, J. Chen, Y. Ren, Z. Pan, L. Zhang, and X. Xing, Phys. Rev. Lett. **116**(2), 027601 (2016).
[9]Y. Huan, X. Wang, Z. Shen, J. Kim, H. Zhou, and L. Li, J. Am. Ceram. Soc. **97**(3), 700 (2014).
[10]S.-E. Park and T. R. Shrout, J. Appl. Phys. **82**(4), 1804 (1997).
[11]M. Davis, M. Budimir, D. Damjanovic, and N. Setter, J. Appl. Phys. **101**(5), 054112 (2007).
[12]Y.-H. Seo, D. J. Franzbach, J. Koruza, A. Benčan, B. Malič, M. Kosec, J. L. Jones, and K. G. Webber, Phys. Rev. B **87**(9), 094116 (2013).
[13]S. Hwang, C. Lynch, and R. McMeeking, Acta Metall. Mater. **43**(5), 2073 (1995).
[14]X. Liu, D. Wu, B. Fang, J. Ding, X. Li, X. Zhao, H. Luo, J.-H. Ko, and C. W. Ahn, Appl. Phys. A **119**(4), 1469 (2015).
[15]M. Suzuki, A. Morishita, Y. Kitanaka, Y. Noguchi, and M. Miyayama, Jpn. J. Appl. Phys. **49**, 09MD09 (2010).
[16]Z. Yu, R. Guo, and A. Bhalla, J. Appl. Phys. **88**, 410 (2000).
[17]R. Sun, X. Zhao, Q. Zhang, B. Fang, H. Zhang, X. Li, D. Lin, S. Wang, and H. Luo, J. Appl. Phys. **109**(12), 124113 (2011).
[18]D. Schneider, W. Jo, J. Rödel, D. Rytz, and T. Granzow, J. Appl. Phys. **116**(4), 044111 (2014).
[19]D. Schneider, J. Rödel, D. Rytz, and T. Granzow, J. Am. Ceram. Soc. **98**(12), 3966 (2015).
[20]H. Deng, X. Y. Zhao, H. W. Zhang, C. Chen, X. B. Li, D. Lin, B. Ren, J. Jiao, and H. S. Luo, CrystEngComm **16**(13), 2760 (2014).
[21]Y. Saito, H. Takao, T. Tani, T. Nonoyama, K. Takatori, T. Homma, T. Nagaya, and M. Nakamura, Nature **432**(7013), 84 (2004).
[22]M. Kosec, B. Malič, A. Benčan, T. Rojac, and J. Tellier, Funct. Mater. Lett. **3**(01), 15 (2010).
[23]K. Chen, G. S. Xu, D. F. Yang, X. F. Wang, and J. B. Li, J. Appl. Phys. **101**(4), 044103 (2007).
[24]J. J. Wang, L. M. Zheng, B. Yang, R. Wang, X. Q. Huo, S. J. Sang, J. Wu, Y. F. Chang, H. P. Ning, and T. Q. Lv, J. Cryst. Growth **409**, 39 (2015).
[25]M. Bah, F. Giovannelli, R. Retoux, J. Bustillo, E. Le Clezio, and I. Monot-Laffez, Cryst. Growth Des. **16**(1), 315 (2016).
[26]Y. Liu, G. Xu, J. Liu, D. Yang, and X. Chen, J. Alloys Compd. **603**, 95 (2014).
[27]H. Uršič, A. Benčan, M. Škarabot, M. Godec, and M. Kosec, J. Appl. Phys. **107**(3), 033705 (2010).
[28]A. Popovič, L. Bencze, J. Koruza, and B. Malič, RSC Adv. **5**(93), 76249 (2015).
[29]Y. Kizaki, Y. Noguchi, and M. Miyayama, Key Eng. Mater. **350**, 85 (2007).
[30]H. Liu, P. Veber, J. Koruza, D. Rytz, M. Josse, J. Rödel, and M. Maglione, CrystEngComm **18**(18), 2081 (2016).
[31]D. Lin, Z. Li, S. Zhang, Z. Xu, and X. Yao, J. Am. Ceram. Soc. **93**(4), 941 (2010).
[32]X. Huo, R. Zhang, L. Zheng, S. Zhang, R. Wang, J. Wang, S. Sang, B. Yang, and W. Cao, J. Am. Ceram. Soc. **98**(6), 1829 (2015).
[33]M. Prakasam, P. Veber, O. Viraphong, L. Etienne, M. Lahaye, S. Pechev, E. Lebraud, K. Shimamura, and M. Maglione, C. R. Phys. **14**(2), 133 (2013).
[34]P. Veber, F. Benabdallah, H. Liu, G. Buse, M. Josse, and M. Maglione, Materials **8**(11), 7962 (2015).
[35]Y. Inagaki, K. Kakimoto, and I. Kagomiya, J. Am. Ceram. Soc. **93**(12), 4061 (2010).
[36]H. J. Trodahl, N. Klein, D. Damjanovic, N. Setter, B. Ludbrook, D. Rytz, and M. Kuball, Appl. Phys. Lett. **93**(26), 262901 (2008).
[37]N. Setter and L. E. Cross, J. Appl. Phys. **51**(8), 4356 (1980).
[38]Y. Huan, X. Wang, J. Koruza, K. Wang, K. G. Webber, Y. Hao, and L. Li, Sci. Rep. **6**, 22053 (2016).
[39]D. Wang, M. Cao, and S. Zhang, J. Am. Ceram. Soc. **94**(11), 3690 (2011).
[40]H. E. Mgbemere, M. Hinterstein, and G. A. Schneider, J. Appl. Crystallogr. **44**(5), 1080 (2011).
[41]V. Y. Topolov, J. Phys.: Condens. Matter **7**(37), 7405 (1995).
[42]R. E. Newnham, *Properties of Materials: Anisotropy, Symmetry, Structure: Anisotropy, Symmetry, Structure* (OUP Oxford, 2004).
[43]W. Ge, C. Luo, Q. Zhang, C. P. Devreugd, Y. Ren, J. Li, H. Luo, and D. Viehland, J. Appl. Phys. **111**(9), 093508 (2012).